

UnWave-Net: Unrolled Wavelet Network for Compton Tomography Image Reconstruction

Ishak Ayad^{1,2(✉,*),} Cécilia Tarpau^{3,} Javier Cebeiro^{4,} and Mai K. Nguyen¹

¹ ETIS (UMR 8051), CY Cergy Paris University, ENSEA, CNRS, France

² AGM (UMR 8088), CY Cergy Paris University, CNRS, France

³ Maxwell Institute for Mathematical Sciences & School of Mathematical and Computer Sciences, Heriot-Watt University, United Kingdom

⁴ ITECA, UNSAM-CONICET, ECyT, Centro de Matemática Aplicada (CEDEMA), Universidad Nacional de San Martín, Argentina
ishak.ayad@cyu.fr

Abstract. Computed tomography (CT) is a widely used medical imaging technique to scan internal structures of a body, typically involving collimation and mechanical rotation. Compton scatter tomography (CST) presents an interesting alternative to conventional CT by leveraging Compton physics instead of collimation to gather information from multiple directions. While CST introduces new imaging opportunities with several advantages such as high sensitivity, compactness, and entirely fixed systems, image reconstruction remains an open problem due to the mathematical challenges of CST modeling. In contrast, deep unrolling networks have demonstrated potential in CT image reconstruction, despite their computationally intensive nature. In this study, we investigate the efficiency of unrolling networks for CST image reconstruction. To address the important computational cost required for training, we propose UnWave-Net, a novel unrolled wavelet-based reconstruction network. This architecture includes a non-local regularization term based on wavelets, which captures long-range dependencies within images and emphasizes the multi-scale components of the wavelet transform. We evaluate our approach using a CST of circular geometry which stays completely static during data acquisition, where UnWave-Net facilitates image reconstruction in the absence of a specific reconstruction formula. Our method outperforms existing approaches and achieves state-of-the-art performance in terms of SSIM and PSNR, and offers an improved computational efficiency compared to traditional unrolling networks.

Keywords: Compton Scatter Tomography · Image reconstruction · Unrolling networks · Wavelet transform.

1 Introduction and Related Works

Computed tomography (CT) is widely used in clinical practice for scanning internal body structures. These devices use collimation to obtain directional x-

* Corresponding author

ray information and mechanical rotation of the source-detector pair around the object to gather complete sets of data. Compton scatter tomography (CST) is an alternative to CT, utilizing Compton physics instead of collimation to obtain directional information of transmitted photons. The directional shift ω observed in Compton scattering correlates with the energy loss of the photon, transitioning from its initial energy E_0 to $E(\omega)$, according to the following one-to-one relation:

$$E(\omega) = \frac{E_0}{1 + \frac{E_0}{mc^2}(1 - \cos \omega)},$$

where $mc^2 = 0.511$ MeV. CST introduces novel possibilities for imaging (assuming the use of energy-resolved sensors), particularly in terms of designing new geometries; for example, compact and/or completely fixed systems can now be contemplated [1–6]. In contrast to traditional CT, certain devices offer scanning configurations with the object positioned outside the system [4, 6–8]. However, CST introduces new challenges in image reconstruction due to data acquisition, which involves the use of generalized Radon transforms on families of circular arcs in 2D. Present literature on this subject is confined to theoretical results providing analytical reconstruction formulas for a limited CST geometries.

With deep learning’s success in CT [9–12] and MRI [13, 14] reconstruction, two main categories emerged: Post-processing methods like FBPConvNet [9] and DuDoTrans [11] treat reconstruction as a denoising task. While effective in addressing artifacts, they often struggle with global information recovery from sparse data. Conversely, unrolling networks have emerged as an enticing technique for image reconstruction [15–21], treating it as an optimization task resulting in an iterative algorithm like gradient descent, and subsequently unrolled into a neural network to learn the regularization terms. However, unrolled networks face two primary challenges: firstly, the difficulty in capturing long-range dependencies due to reliance on locally-focused regularization terms using CNNs; secondly, unrolled networks consist of a cascade of network layers to mimic the iterative reconstruction process, leading to high computational costs.

In this paper, we explore unrolling networks [22] efficiency for CST image reconstruction. Furthermore, to mitigate memory and computational costs of unrolling networks, we introduce UnWave-Net, a novel deep unrolled network incorporating a wavelet-based regularization term. Our approach employs a discrete wavelet transform on the input features [23, 24], decomposing them into low-frequency (LL) and high-frequency (LH, HL, HH) components across four sub-bands. The regularization term is specifically applied to the low-frequency features, resulting in a significant reduction in learning and inference times while preserving quality. To demonstrate the efficacy of UnWave-Net, we consider a non-collimated circular CST (NCCCST) system, comprised of a source and sensors positioned on a circular ring. The analytic inversion of the corresponding Radon transform remains an open problem. We illustrate that the UnWave-Net represents a compelling method for image reconstruction in NCCCST, achieving state-of-the-art results in both training and inference speed, along with superior performance in quantitative metrics. The main contributions of this paper are:

1. UnWave-Net, a wavelet unrolled network for CST image reconstruction leveraging wavelet subbands' dimensional reduction to expedite inference.
2. Achievement of state-of-the-art results in training and inference times, along with superior quantitative performance through experiments conducted on a CST modality, which lacks an inverse analytic formula for image reconstruction.

2 Modelling of the Non-Collimated Circular CST

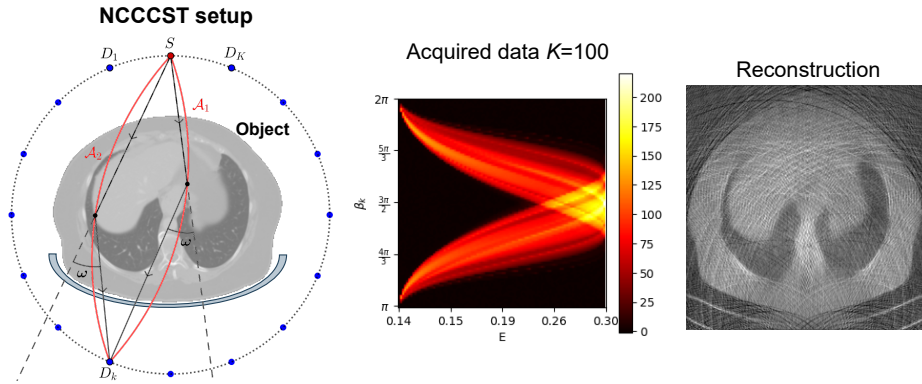


Fig. 1. NCCCST setup. Left: the dotted circle represents the ring containing point-like blue detectors D_k , with the red source S . Center: measured data. Right: reconstruction using pseudo-inversion of the data exhibits severe artifacts.

The NCCCST system consists of a source S and K fixed uncollimated detectors $D_k, k \in \{1, \dots, K\}$ placed on a radius of $P/2$ including the source. Detectors are non-collimated and energy-resolved. The scanned object is within the ring, and the source has a plate collimator confining photons to a plane, defining, thus, a 2D scanning slice (see Fig. 1). NCCCST inherits advantages from its predecessor CCST [4, 5], such as non-moving components and a compact design. First-order scattered photons recovered by a detector D_k at the same energy $E(\omega)$ correspond to scattering sites on one of two circle arcs with S and D_k as endpoints, subtending the angle $(\pi - \omega)$. An example of such a pair of scanning arcs is depicted in Fig. 1. The data model considers only first-order scattering, with higher orders treated as noise. Attenuation effects are neglected. In contrast to CCST [5], NCCCST doesn't determine if the scattering site lies on circle arc \mathcal{A}_1 or \mathcal{A}_2 given a scattering angle ω .

In the following calculations, the source S is placed at the origin of the coordinate system. Let f be a non-negative function with compact support inside a disc of diameter P centred at $O = (0, -P/2)$. The Radon-type model mapping

f to its integrals over the family of double circular arcs $\mathcal{A}_1 \cup \mathcal{A}_2$ is given by:

$$\mathcal{R}f(\omega, \beta_k) = \int_{-\infty}^{\infty} \left[\int_{\beta_k}^{\beta_k + \omega} f(r, \theta) \mathcal{K}(\omega, \beta_k; r, \theta) d\theta + \int_{\beta_k - \omega}^{\beta_k} f(r, \theta) \mathcal{K}(-\omega, \beta_k; r, \theta) d\theta \right] dr, \quad (1)$$

where $\mathcal{K}(\omega, \beta_k; r, \theta) = \rho(\omega, \beta_k) \delta(r - \rho(\omega, \beta_k) \cos(\theta - \phi(\omega, \beta_k)))$ is a delta kernel defining the scanning circle arcs with diameter $\rho(\beta_k, \omega) = P \cos(\beta_k + \frac{\pi}{2}) / \sin(\omega)$ and relative angle $\phi(\beta_k, \omega) = \beta_k + \omega - \pi/2$ to the x -axis. Variables are the scattering angle ω , the angle subtended by the detector β_k , and the polar variables (r, θ) . Function f represents the electronic density of the object and $\mathcal{R}f(\omega, \beta_k)$ is the data measured by detectors. An example of collected data is presented in Fig. 1. Currently, neither inverse formulas nor inversion results are known for the model on pairs of circles (Eq. 1). This is mainly due to the lack of shift or rotational invariance in the direct operator, motivating our work to find a solution for image reconstruction, i.e., the inversion of Eq. 1.

3 Methodology

3.1 Related Theories

Inverse Problem Formulation. NCCCST image reconstruction problem can be mathematically formalized as the solution to a linear equation in the form of:

$$\mathbf{y} = \mathbf{A}\mathbf{x}, \quad (2)$$

where $\mathbf{x} \in \mathbb{R}^n$ represents the object to reconstruct ($n = h \times w$), and $\mathbf{y} \in \mathbb{R}^m$ denotes the data ($m = K \times N_E$), where K is the number of detectors and N_E is the number of finite elements in the energy domain $[E(\pi), E_0]$. $\mathbf{A} \in \mathbb{R}^{n \times m}$ is the discrete forward model. The objective is to recover the object \mathbf{x} from the observed data \mathbf{y} . Since CST image reconstruction deals with an ill-posed inverse problem, pseudo-inversion is insufficient for qualitative reconstruction (see Fig. 1). Iterative reconstruction algorithms are employed to minimize a regularized objective function with an L^2 norm constraint:

$$\hat{\mathbf{x}} = \arg \min_{\mathbf{x}} J(\mathbf{x}) = \frac{\lambda}{2} \|\mathbf{A}\mathbf{x} - \mathbf{y}\|_2^2 + \mathcal{F}(\mathbf{x}), \quad (3)$$

where $\mathcal{F}(\mathbf{x})$ is the regularization term. Initially, ill-posed problems were addressed using optimization techniques like the truncated singular value decomposition (SVD) algorithm [25] or iterative approaches such as algebraic reconstruction technique (ART) [26]. Additionally, techniques like total variation [27] and Tikhonov regularization [28] can improve the reconstructions.

Deep Unrolling Networks. Assuming that \mathcal{F} is differentiable and convex, gradient descent can be used to solve Eq. 3:

$$\mathbf{x}_{t+1} = \mathbf{x}_t - \alpha(\lambda \mathbf{A}^\dagger (\mathbf{A}\mathbf{x}_t - \mathbf{y}) + \nabla_{\mathbf{x}} \mathcal{F}(\mathbf{x}_t)), \quad (4)$$

where α is the step size (neglected for redundancy with the learned parameters), and \mathbf{A}^\dagger is the pseudo-inverse. Optimization limitations, like manual parameter selection, are tackled by recent deep learning methods [17,21]. By allowing terms in Eq. 4 to be iteration dependent, the gradient descent iteration becomes:

$$\mathbf{x}_{t+1} = \mathbf{x}_t - \lambda_t \mathbf{A}^\dagger (\mathbf{A} \mathbf{x}_t - \mathbf{y}) + \mathcal{G}(\mathbf{x}_t), \quad (5)$$

where \mathcal{G} is a learned mapping representing the gradient of the regularization term. Finally, Eq. 5 is unrolled into a deep recurrent neural network to learn the optimization parameters and the regularization term.

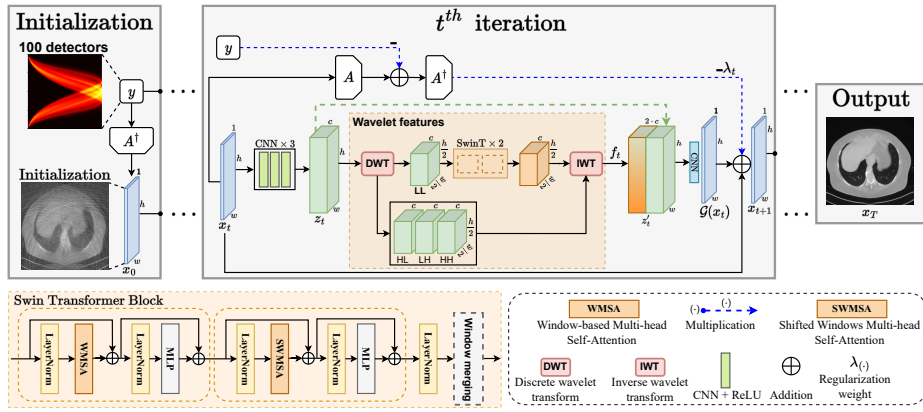


Fig. 2. Overall structure of the proposed UnWave-Net for NCCCT reconstruction. The method utilizes wavelet transform to reduce computational complexity.

3.2 The proposed UnWave-Net

Recent studies on unrolling networks have explored various representations of the regularization term gradient (denoted as \mathcal{G} in Eq. 5), from conv-nets [13, 17, 29] to attention-based networks [14, 21]. As deep learning models grow in complexity, the representation of the regularization term gradient becomes more computationally and memory-intensive [22]. To mitigate this, we introduce UnWave-Net, a novel unrolling network that leverages the wavelet transform to represent the regularization term gradient. Recently, the wavelet transform has been widely used to reduce the complexity of deep learning models, such as diffusion probabilistic models [23], or in NeRF models for generalizable, high-quality synthesis [24]. Inspired by this, we apply a CNN layer to the input image $\mathbf{x}_t \in \mathbb{R}^{h \times w \times 1}$ at iteration t to obtain $\mathbf{z}_t \in \mathbb{R}^{h \times w \times c}$ feature map, which is then transformed into wavelet coefficients $\mathbf{w}_t \in \mathbb{R}^{\frac{h}{2} \times \frac{w}{2} \times 4 \cdot c}$. The LL-frequencies undergo Swin Transformer processing [30] to capture long-range dependencies, while the HL, LH, and HH frequencies remain unchanged. After inverse wavelet transformation, the

new feature map $\mathbf{f}_t \in \mathbb{R}^{h \times w \times c}$ is concatenated with \mathbf{z}_t to yield final feature map $\mathbf{z}'_t = \text{cat}(\mathbf{z}_t, \mathbf{f}_t) \in \mathbb{R}^{h \times w \times 2 \cdot c}$. Lastly, \mathbf{z}'_t passes through a CNN layer to produce the regularization term gradient $\mathcal{G}(\mathbf{x}_t) \in \mathbb{R}^{h \times w \times 1}$. The overall architecture of the proposed UnWave-Net is depicted in Fig. 2. The network takes as inputs the acquired data \mathbf{y} and the corresponding pseudo-inverse reconstruction $\mathbf{A}^\dagger \mathbf{y}$. It consists of T iterations, each incorporating a wavelet regularization term.

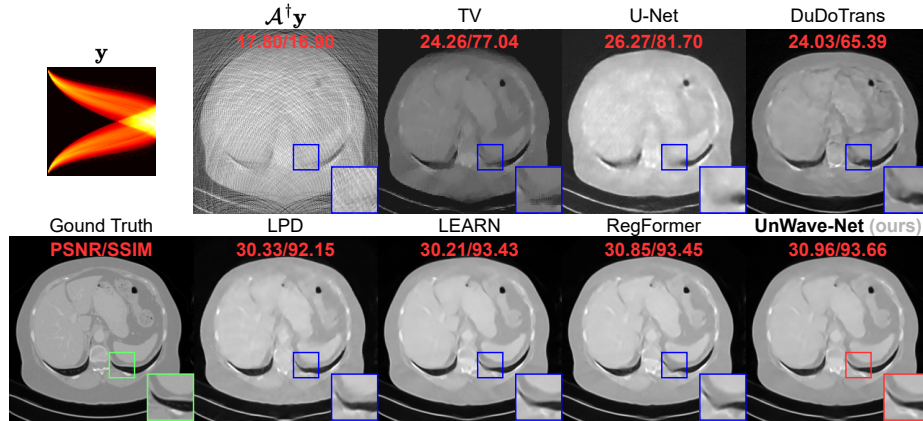


Fig. 3. Visual comparison with noisy data and $K = 100$. The cropped region highlights the superior artifact suppression of our UnWave-Net compared to RegFormer.

4 Experiments

4.1 Experimental Setup

Dataset and Evaluation metrics. We evaluate our method on the AAPM dataset [31], consisting of 2378 full-dose CT images with 3mm thickness from 10 patients. In line with standard practices [11, 17, 21], we employ peak signal-to-noise ratio (PSNR) and structural similarity index measure (SSIM) for quantitative evaluation.

Implementation and Training details. The AAPM dataset is divided into 1920 training images from 8 patients, 244 validation images from 1 patient, and 214 test images from the remaining patient, all resized to 256×256 . The considered NCCCST is made of $K \in \{100, 150\}$ detectors of energy resolution $\Delta E = 0.0016$ MeV. The source is assumed to be mono-energetic of energy $E_0 = 0.3$ MeV. The forward operator is simulated by discretizing Eq. 1. To mimic real-world CT scanning, mixed noise is applied to the acquired data, comprising 5% Gaussian noise and Poisson noise with an intensity of 1×10^6 . Model training involves 50 epochs using 4 Nvidia Tesla V100 GPUs (32GB RAM). The AdamW

optimizer [32] with a learning rate of 1×10^{-4} and weight decay 1×10^{-2} is used, along with MSE loss and a batch size of 1. A learning rate decay factor of 0.1 is applied after 40 epochs. The unrolling iterations for UnWave-Net are set to $T = 16$, and a Haar wavelet transform with a feature map depth of 48 is employed for regularization. The sizes of the convolution kernel are 5×5 . For the SwinT model, a window size of 8 and a depth of 2 are utilized.

State-of-the-art baselines. We compare UnWave-Net with Chambolle-Pock’s algorithm using a handcrafted total variation (TV) regularizer and several state-of-the-art CT reconstruction models: (1) post-processing methods, namely U-Net [9] and DuDoTrans [11]; (2) deep unrolling networks, including LPD [15], LEARN [17], and RegFormer [21]. It is important to note that the FBP operators in these methods are replaced by pseudo-inverse reconstruction due to the lack of an analytical solution for the NCCCST problem. To ensure fair comparison, we use authors’ code or meticulously implement methods based on their papers.

Table 1. Quantitative evaluation on AAPM of state-of-the-art methods (PSNR in dB and SSIM in %). **Bold:** Best, under: second best.

Method	No noise				With noise			
	$K = 150$		$K = 100$		$K = 150$		$K = 100$	
	PSNR \uparrow	SSIM \uparrow	PSNR \uparrow	SSIM \uparrow	PSNR \uparrow	SSIM \uparrow	PSNR \uparrow	SSIM \uparrow
Pseudo-inverse	19.52	21.90	18.21	17.26	19.43	21.44	18.17	17.08
TV	26.61	80.56	25.33	78.31	26.54	80.51	25.27	78.19
U-Net [9]	28.32	83.59	27.14	81.47	28.03	83.93	27.36	82.58
DuDoTrans [11]	29.16	81.96	27.32	80.08	28.99	81.46	27.36	79.74
LPD [15]	32.07	94.05	31.48	92.86	31.43	92.72	31.40	91.83
LEARN [17]	31.92	<u>95.11</u>	31.90	94.08	31.63	93.66	<u>32.16</u>	92.95
RegFormer [21]	<u>32.45</u>	95.02	<u>32.54</u>	94.22	<u>32.11</u>	<u>93.80</u>	31.83	<u>92.98</u>
UnWave-Net (ours)	32.86	95.12	32.73	<u>94.18</u>	32.48	93.91	32.44	93.07

4.2 Comparison with state-of-the-art methods

Quantitative and Visual comparisons. We evaluate our model against state-of-the-art baselines employing two different numbers of detectors, $K \in \{100, 150\}$, and considering two levels of noise: noise-free and noisy data. The summarized results are presented in Table 1. Our approach, UnWave-Net, consistently achieves state-of-the-art performance across all scenarios. It surpasses the second-best baseline, RegFormer, with an average improvement of (+0.03% SSIM, +0.3 dB PSNR) and (+0.1% SSIM, +0.49 dB PSNR) under noise-free and noisy conditions, respectively. Visual results are depicted in Fig. 3, where U-Net, DuDoTrans, and LPD produce blurry images with noticeable artifacts. Although RegFormer and LEARN perform adequately, they lack detail in the

lung and aorta regions. In contrast, UnWave-Net consistently generates detailed, high-quality images.

Efficiency comparison. The results in Table 2, conducted on one V100 GPU, show that UnWave-Net is computationally more efficient than gradient descent-based unrolling networks, outperforming LEARN and RegFormer with speedups of $1.36\times$ and $1.31\times$, respectively. Moreover, UnWave-Net utilizes less memory than RegFormer, reducing memory usage by $1.13\times$, approaching the efficiency of LPD. Additionally, our method requires only 16 unrolling iterations compared to 30 for LEARN and 18 for RegFormer, all while achieving superior performance.

Table 2. Efficiency comparison of state-of-the-art methods with $K = 100$.

Method	Unrolled	#Iters	Epoch time (s)	#Params (M)	Memory (GB)	Inference time (ms)
TV	\times	500	-	-	-	5600
U-Net [9]	\times	-	80	31.1	3.94	12.7
DuDoTrans [11]	\times	-	115	15.0	3.80	27.5
LPD [15]	\checkmark	10	370	0.25	3.63	86.4
LEARN [17]	\checkmark	30	1600	3.50	3.64	305
RegFormer [21]	\checkmark	18	1710	4.84	4.22	294
UnWave-Net (ours)	\checkmark	16	1270	2.80	3.72	224

4.3 Ablation Study

To assess how the number of unrolling iterations affects UnWave-Net’s performance, we conducted an ablation study on the AAPM dataset with $K = 100$. Fig. 4a and Fig. 4b illustrate that even with $T \leq 16$, UnWave-Net achieves higher PSNR and SSIM metrics compared to RegFormer and LEARN. This underscores the effectiveness of UnWave-Net over other gradient descent-based unrolling networks. Additionally, UnWave-Net exhibits significantly lower time costs than RegFormer and LEARN, as shown in Fig. 4c, even when $T = 20$. This showcases the efficiency of our method in terms of inference time.

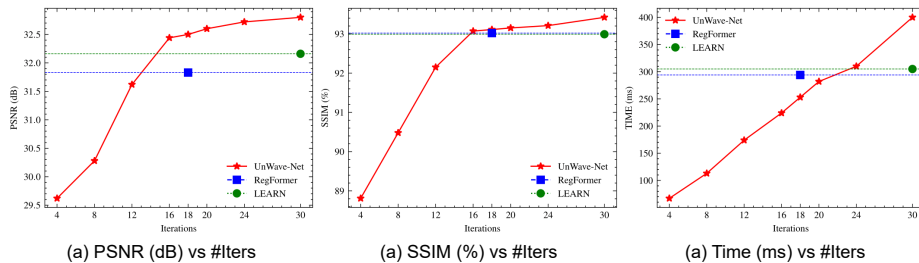


Fig. 4. Ablation on the number of unrolling iterations. Quantitative and efficiency comparisons of our UnWave-Net against RegFormer and LEARN.

5 Conclusion

In this paper, we present UnWave-Net, a wavelet-based deep unrolled network tailored for CST imaging. Through extensive experimentation on a stationary CST system with circular geometry (i.e., NCCCST), UnWave-Net demonstrates superior performance in both image quality and reconstruction speed, positioning it as a state-of-the-art solution in this domain. Notably, our study underscores the adaptability and effectiveness of established unrolling networks in addressing novel imaging challenges, showcasing their versatility and broad applicability. Moreover, we emphasize the practical advantage of UnWave-Net’s robustness to noisy data, enhancing its feasibility in real-world scenarios. We envision UnWave-Net as a promising method for CST imaging with potential extensions to other imaging modalities. Nonetheless, it is essential to acknowledge that our approach inherits the inherent drawback of deep unrolled networks, particularly in terms of prolonged training time compared to post-processing methods. Future research efforts will focus on addressing these limitations.

6 Acknowledgments

This work was granted access to the HPC resources of IDRIS under the allocation 2021-[AD011012741] / 2022-[AD011013915] provided by GENCI and supported by DIM Math Innov funding.

References

1. Norton, S.J.: Compton-scattering tomography with one source and one detector: a simple derivation of the filtered-backprojection solution. *Inverse Problems in Science and Engineering* pp. 1–12 (2019)
2. Truong, T.T., Nguyen, M.K.: Radon transforms on generalized Cormack’s curves and a new Compton scatter tomography modality. *Inverse Problems* **27** (2011)
3. Tarpau, C., Cebeiro, J., Morvidone, M.A., Nguyen, M.K.: A new concept of Compton scattering tomography and the development of the corresponding circular Radon transform. *IEEE TRPMS* **4**, 433–440 (2020)
4. Tarpau, C., Nguyen, M.K.: Compton scattering imaging system with two scanning configurations. *Journal of Electronic Imaging* **29** (2020)
5. Tarpau, C., et al.: Analytic inversion of a Radon transform on double circular arcs with applications in Compton scattering tomography. *IEEE TCI* **6**, 958–967 (2020)
6. Cebeiro, J., et al.: On a three-dimensional Compton scattering tomography system with fixed source. *Inverse Problems* (2021)
7. Webber, J., Miller, E.L.: Compton scattering tomography in translational geometries. *Inverse Problems* **36** (2020)
8. Truong, T.T., Nguyen, M.K.: Recent Developments on Compton Scatter Tomography: Theory and Numerical Simulations. *IntechOpen* (2012)
9. Jin, K.H., et al.: Deep convolutional neural network for inverse problems in imaging. *IEEE Transactions on Image Processing* **26**, 4509–4522 (2017)
10. Zhang, Z., et al.: A sparse-view CT reconstruction method based on combination of DenseNet and deconvolution. *IEEE TMI* **37**, 1407–1417 (2018)

11. Wang, C., et al.: DuDoTrans: Dual-domain transformer for sparse-view CT reconstruction. In: *Machine Learning for Medical Image Reconstruction*. pp. 84–94 (2022)
12. Li, Z., et al.: Learning to distill global representation for sparse-view CT. In: *ICCV*. pp. 21196–21207 (2023)
13. Sriram, A., et al.: End-to-End variational networks for accelerated MRI reconstruction. In: *MICCAI*. pp. 64–73 (2020)
14. Fabian, Z., Tinaz, B., Soltanolkotabi, M.: HUMUS-Net: Hybrid unrolled multi-scale network architecture for accelerated MRI reconstruction. In: *NeurIPS* (2022)
15. Adler, J., Öktem, O.: Learned primal-dual reconstruction. *IEEE TMI* **37**, 1322–1332 (2018)
16. Harshit, G., et al.: CNN-based projected gradient descent for consistent CT image reconstruction. *IEEE TMI* **37**, 1440–1453 (2018)
17. Chen, H., et al.: LEARN: Learned experts’ assessment-based reconstruction network for sparse-data CT. *IEEE TMI* **37**, 1333–1347 (2018)
18. Wang, J., et al.: ADMM-based deep reconstruction for limited-angle CT. *Physics in Medicine & Biology* **64** (2019)
19. Dianlin, H., et al.: DIOR: Deep iterative optimization-based residual-learning for limited-angle CT reconstruction. *IEEE TMI* **41**, 1778–1790 (2022)
20. Jinxi, X., Yonggui, D., Yunjie, Y.: FISTA-Net: Learning a fast iterative shrinkage thresholding network for inverse problems in imaging. *IEEE TMI* **40**, 1329–1339 (2021)
21. Xia, W., et al.: Transformer-based iterative reconstruction model for sparse-view CT reconstruction. In: *MICCAI*. pp. 790–800 (2022)
22. Monga, V., Li, Y., Eldar, Y.C.: Algorithm unrolling: Interpretable, efficient deep learning for signal and image processing. *IEEE Sig. Proc. Mag.* **38**(2), 18–44 (2021)
23. Phung, H., Dao, Q., Tran, A.: Wavelet diffusion models are fast and scalable image generators. In: *CVPR*. pp. 10199–10208 (2023)
24. Xu, M., et al.: Wavenerf: Wavelet-based generalizable neural radiance fields. In: *ICCV*. pp. 18149–18158 (2023)
25. Rui, L., et al.: Singular value decomposition-based 2D image reconstruction for computed tomography. *Journal of X-ray science and technology* **25**, 113–134 (2017)
26. Avinash, K., Malcolm, S.: *Principles of Computerized Tomographic Imaging*. Society for Industrial and Applied Mathematics (2001)
27. Tsutomu, G., Yukio, K.: Use of a Total Variation minimization iterative reconstruction algorithm to evaluate reduced projections during digital breast tomosynthesis. *BioMed Research International* pp. 1–14 (2018)
28. Peng, C., Rodi, W.L., Töksöz, M.N.: *A Tikhonov Regularization Method for Image Reconstruction*. Springer US (1993)
29. Yi, Z., et al.: LEARN++: Recurrent dual-domain reconstruction network for compressed sensing CT. *IEEE TRPMS* **7**, 132–142 (2023)
30. Liu, Z., et al.: Swin transformer: Hierarchical vision transformer using shifted windows. In: *ICCV*. pp. 10012–10022 (2021)
31. McCollough, C.: TU-FG-207A-04: Overview of the low dose CT grand challenge. *Medical Physics* **43**, 3759–3760 (2016)
32. Loshchilov, I., Hutter, F.: Decoupled Weight Decay Regularization. arXiv preprint arXiv:1711.05101 (2017)